1   # Engineering green-to-blue emitting CsPbBr$_3$

2   # quantum-dot films with efficient ligand passivation

3   Maowei Jiang, [†] Zhanhao Hu, [†] Zonghao Liu, Zhifang Wu, Luis K. Ono and Yabing Qi*

4   Energy Materials and Surface Sciences Unit (EMSSU), Okinawa Institute of Science and

5   Technology Graduate University (OIST), 1919-1 Tancha, Onna-son, Okinawa 904-0495, Japan

6   **Corresponding Author**

7   *Corresponding author: Yabing Qi, E-Mail: Yabing.Qi@OIST.jp

8   **Contributions**

9   [†]M.J. and Z.H. contributed equally to this work.

10   ABSTRACT: A series of challenging issues such as field-driven spectra drift for the $CsPbCl_xBr_{3-}$

11    $_x$ system and mixed phases in quasi-two-dimensional structures still exist when devising blue-

12   emitting perovskites. In this paper, the $CsPbBr_3$ quantum-dot (QD) system is proposed to overcome

13   the above challenges. However, to date the $CsPbBr_3$ QD films with tunable colors from green to

14   blue still cannot be achieved yet using existing methods. Herein, a simple one-step spin-coating

15   route incorporated with efficient ligand passivation is developed to realize this. The size restriction

16   of $CsPbBr_3$ QDs is enabled by a diammonium ligand, propane-1,3-diammonium bromide (PDAB).

17   A mixed ligand system of phenethylammonium bromide (PEAB) with PDAB is further explored

18   to enhance their optical performance. The $CsPbBr_3$ QDs experience a second growth process upon

19   controlled air exposure, which is utilized to realize their size control and emission wavelength

20   tunability. The $CsPbBr_3$ QDs-based devices exhibit no spectra drift in electroluminescence under

21   voltage bias.

22   **TOC GRAPHICS**

23

2
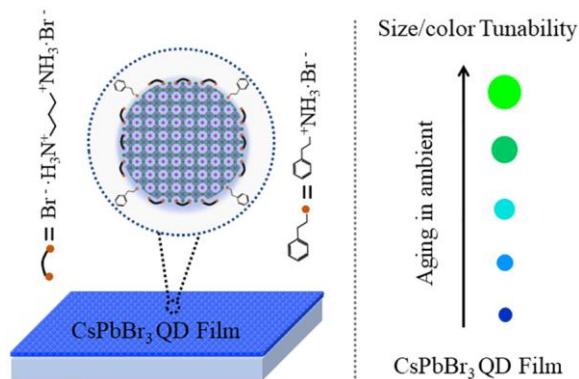
24   Solution-processed lead halide perovskite $APbX_3$ materials (A represents monovalent cations and

25   X represents halide anions) have attracted much attention for their potential applications in solar

26   cells, light-emitting diodes (LEDs), photodetectors, lasers, etc.[1-5] For luminescence related studies,

27   for example, green-, red- and near-infrared- perovskite LEDs have gained much progress with high

28   external quantum efficiency.[6-10] However, the study of perovskites with emissions shifting from

29   green to blue region (500 - 450 nm) has remained challenging due to their limited photo- and

30   electrical- stability.[11-12]

31   Generally, two approaches, namely compositional engineering and quantum-confinement

32   engineering, have been employed to devise blue emitting perovskites, taking $CsPbBr_3$ as a typical

33   example.[13-14] In the compositional engineering approach, mixing Cl^- in $CsPbBr_3$ has been proven

34   to be an efficient way to adjust its bandgap.[15-18] However, the spectrum drift under voltage bias in

35   this Cl-alloyed system has been an obstacle for their practical applications.[13, 19] The other strategy

36   is to reduce the dimensionality of perovskites within the quantum-confinement regime. Thereinto,

37   one popular way is to form quasi-two-dimensional (quasi-2D) structures, which can indeed result

38   in blue-shifted photoluminescence (PL) spectral features.[20-21] However, for electroluminescence

39   (EL) applications of the quasi-2D structures with mixed phases, the blue-emitted region may

40   completely vanish due to charge transfer from low-dimensional 2D perovskites to high-

41   dimensional 2D/3D perovskites. In most cases, the reported quasi-2D $CsPbBr_3$ system only results

42   in green EL emissions.[22-24]

43   Another important class of luminescent perovskites are nanocrystal systems via colloidal

44   synthesis. Perovskite nanocrystals exhibit a high PL quantum yield benefitted from space-confined

45   exciton recombination and well-defined surface passivation.[25-28] To date, however, almost all the

46   reports based on colloidal $CsPbBr_3$ nanocrystals are devoted to green EL emissions.[29-31] Further

47 size decrease of $CsPbBr_3$ nanocrystals into the quantum confinement region may result in blue-

48 emitting $CsPbBr_3$ QDs. $CsPbBr_3$ QDs with blue emissions have been produced via the colloidal

49 synthesis method; however, the excess long-chain acid and amine ligands, inorganic salts such as

50 $ZnBr_2$ or organic long-chain ammonium halide are needed in the synthesis and subsequent

51 purification processes to sustain their size stably.[26, 32-34] These excessive additives are not ideal for

52 device fabrication due to their poor charge transport properties.[35-36] Furthermore, when depositing

53 the $CsPbBr_3$ QDs solution onto a substrate, the film formation process from the colloidal solution

54 may result in severe aggregation, which leads to size increase of $CsPbBr_3$ QDs. Accordingly, the

55 blue emissions below 500 nm in EL have not been realized for colloidal $CsPbBr_3$ QD based

56 films.[18, 37]

57 Considering all the disadvantages encountered in Cl-alloyed systems, quasi-2D systems, and

58 colloidal $CsPbBr_3$ QD systems, it is imperative to perform fundamental studies as well as to search

59 for alternative approaches to realize stable blue-shifted emissions of $CsPbBr_3$. We propose the

60 $CsPbBr_3$ QDs composed film system to deal with the above challenges. Indeed, the concept of

61 $CsPbBr_3$ QD films has been attracting much attention of researchers,[12, 37] but unfortunately the

62 $CsPbBr_3$ QD films still cannot be produced successfully with the existing methods to date. The

63 efforts to produce $CsPbBr_3$ QD films should be made prior to exploring their properties and

64 applications.

65 In this work, we developed a new methodology of preparing spin-coated blue $CsPbBr_3$ QD films

66 based on the enhanced ligand passivation (Figure 1a). It's known that the crystallization of 3D or

67 quasi-2D perovskite thin films can be realized via simple spin-coating method from the precursor

68 solution after annealing.[7, 13] Following this route, the core question is how to restrict the growth of

69 $CsPbBr_3$ domains during the spin-coating and annealing processes? Hints come from reports

70   showing that formation of quasi-2D $CsPbBr_3$ structures is induced by the passivation effect of

71   organic ammonium ligands such as butylammonium bromide and phenethylammonium bromide

72   (PEAB).[20-21] The ammonium groups of these ligands directly coordinate with perovskite crystals,

73   while the opposite organic end groups terminate the further growth of perovskite crystals.

74   However, the hydrophobicity of these organic end groups in a polar precursor solution leads to

75   oriented stacks so that the layered structures are formed. The hydrophobic interaction of the

76   organic end groups can be minimized chemically by increasing their polarity. In view of this, we

77   tried to adopt a short-chain diammounium salt as the ligand, namely propane-1,3-diammonium

78   bromide (PDAB). We assume that the two primary ammonium groups of PDAB synergistically

79   passivate the surface of $CsPbBr_3$ crystals. Also, this di-bromide ligand may provide a halide-rich

80   environment, resulting in defect healing of halide vacancies. Inspired by these ideas, we

81   successfully fabricated $CsPbBr_3$ QDs-based thin films with tunable PL and EL from green to blue

82   colors. To further enhance their optical performance, a mixed ligand system of PDAB and PEAB

83   was further developed. The PL and EL properties of $CsPbBr_3$ QD films were studied to explore

84   their humidity-induced size control of $CsPbBr_3$ QDs and their spectra-stability under voltage bias.

85   The $CsPbBr_3$ thin films were deposited directly by spin-coating the precursor solution (prepared

86   by mixing 1.1 mmol $PbBr_2$, 1 mmol CsBr and certain molar amount of ligands in dimethyl

87   sulfoxide solvent) onto poly(3,4-ethylenedioxythiophene):poly(styrenesulfonate) coated indium-

88   doped tin oxide (ITO/PEDOT:PSS) substrates, followed by annealing (Figure 1a). The $CsPbBr_3$

89   QDs could be synthesized in situ and patterned with a form of thin film, which is named as $CsPbBr_3$

90   QD film below. Our procedure has the advantage of the simplicity for the preparation of $CsPbBr_3$

91   QD films when compared to the traditional colloidal synthesis route, which requires the separated

92   steps of synthesis, purification, and thin film processing. Note that when exploring optoelectronic

93   device applications based on colloidal CsPbBr$_3$ QDs, the purification and film formation processes

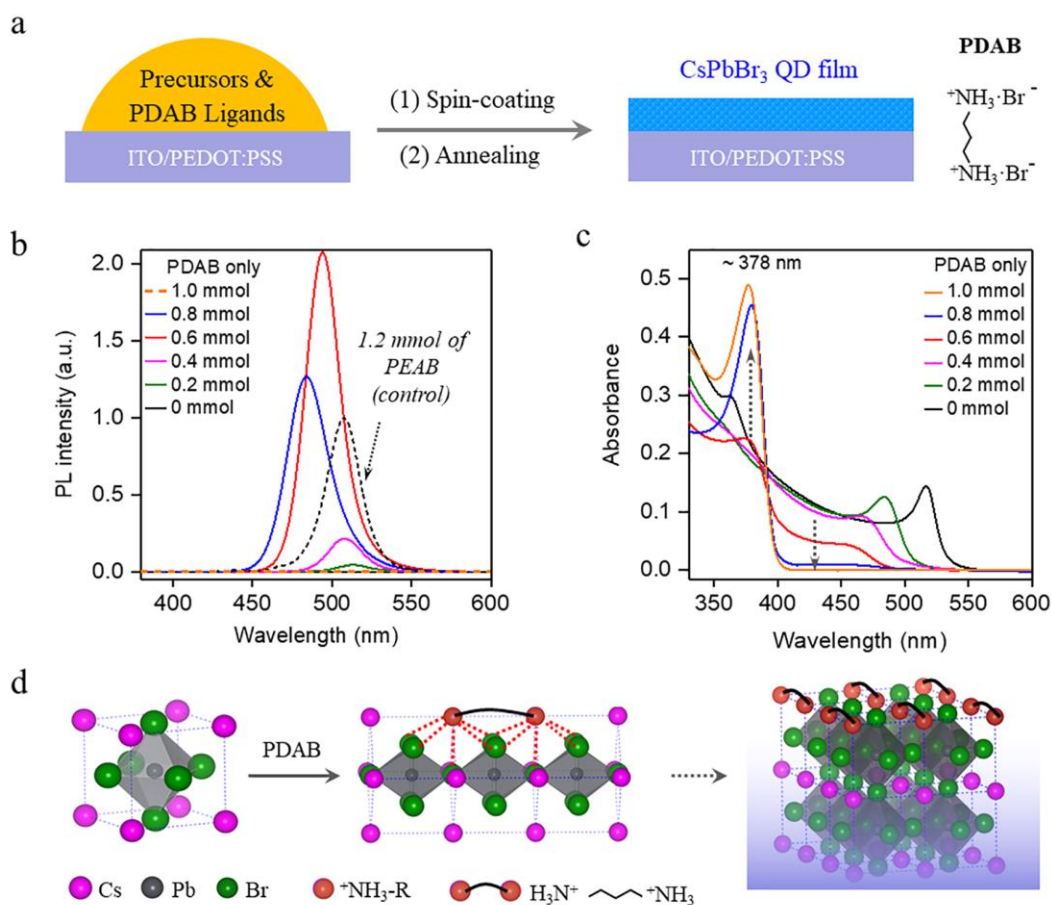94   may result in destructive effects on their morphology and optoelectronic properties as reported.[36-

95   37]

96

Figure 1. PDAB ligands assisted formation of CsPbBr$_3$ QD films. (a) Schematic illustration of one step spin-coating route to prepare CsPbBr$_3$ QD films. The molecular structure of PDAB is provided on the right panel. (b) PL and (c) UV-vis spectra for CsPbBr$_3$ thin films processed with different molar amounts of PDAB. The PL curves in (b) are normalized by the maximal PL intensity of CsPbBr$_3$ thin film processed with 1.2 mmol of PEAB (dot-line). (d) Schematic illustration of the proposed passivation mechanism of PDAB on CsPbBr$_3$. The red dot-lines imply the interaction of negative bromide ions and positive ammonium groups of PDAB.

104 For the control experiment without any ligand, weak PL is detected with an emission of bulk

105 $CsPbBr_3$ at 520 nm (Figure 1b), and the time-resolved PL measurement shows a fast decay lifetime

106 for this Pb-excess film inferring a high density of defects (Figure S1).[9, 38] To restrict the growth of

107 $CsPbBr_3$ crystal domains, initial attempts were conducted with the widely used ammonium

108 ligands, typically PEAB. According to the reports[14, 22] and our own results (Figures 1b and S2),

109 the PEAB ligands can enhance the PL intensity of $CsPbBr_3$ to some extent, but cannot blue-shift

110 the PL wavelength below 500 nm without the occurrence of quasi-2D structures.

111 In contrast, the PDAB ligands gave impressive results in blue-shifting the PL wavelength. Once

112 the PDAB ligands are added into the precursor solution, the PL peak of the produced $CsPbBr_3$ QD

113 film is dramatically blue-shifted (Figure 1b). Moreover, the PL intensity of the $CsPbBr_3$ QD film

114 is greatly enhanced, and the corresponding PL lifetime is prolonged (Figures 1b and S1). These

115 results reveal that the surface defect density of the $CsPbBr_3$ QD film could be effectively reduced

116 via the surface passivation strategy of PDAB ligands, thus the non-radiative recombination of

117 $CsPbBr_3$ QDs could be inhibited.[13, 39] With 0.6 mmol of PDAB, the $CsPbBr_3$ QD film shows a

118 maximal PL intensity. Relatively, we tried to evaluate the light-emitting intensities of our films by

119 comparison with a control sample, namely the 1.2 mmol PEAB processed $CsPbBr_3$ thin film,

120 considering that PEAB has been one of the most popular ligands to increase the PL quantum yield

121 and to enhance the LEDs performance of $CsPbBr_3$ thin film.[13, 22] Note that the two cases of 0.6

122 mmol PDAB and 1.2 mmol PEAB have the same molar amounts of ammonium and bromide ions,

123 but the former shows much more blue-shifted PL peak and enhanced PL intensity than the latter.

124 Thus, PDAB ligands can provide efficient passivation for $CsPbBr_3$ and restrict the growth of

125 $CsPbBr_3$ nanodomains within the quantum-confinement regime. Although the absolute PL

126 quantum yield information of our films cannot be provided currently in this report, the above

7

127   results exactly demonstrate great potential of PDAB ligands to achieve bright blue-emitting

128   $CsPbBr_3$ thin films, considering their comparison results with the films processed without any

129   ligands or with PEAB ligands.

130   As the amount of PDAB ligands are increased from 0 mmol to 0.8 mmol, the PL wavelength

131   undergoes a dramatic blue-shift from 521 nm to 483 nm, which is consistent with the blue-shifted

132   UV-vis spectra (Figure 1c). In Figure 1c, it's worthy of pointing out that the first exciton absorption

133   peak of the $CsPbBr_3$ QD films cannot be clearly observed as more PDAB is introduced, and this

134   phenomenon has been also reported in some other monodisperse and polydisperse colloidal

135   $CsPbBr_3$ QDs solution systems[33, 40] or in quantum confined quasi-2D perovskite film systems with

136   higher dimensionality.[11, 13-14] In addition, for the X-ray diffraction (XRD) data in Figure S4, the

137   nanosized $CsPbBr_3$ crystal domains are further demonstrated by the decreased peak intensity and

138   the broadened peak full-width at half-maximum (FWHM) gradually as more PDAB ligands are

139   introduced into the system. On the other hand, no peaks ascribed to 2D perovskites could be

140   observed in our films, as evidenced in the PL, UV-vis and XRD spectra (Figures 1b-c, S3 and S4).

141   The absorption in 400 – 500 nm in Figure 1c is contributed by $CsPbBr_3$. As the amount of PDAB

142   is increased over 0.4 mmol, the absorbance in this region decreases. Correspondingly, a new

143   absorption peak around 378 nm occurs, which is obviously observed for the 0.8 mmol and 1.0

144   mmol PDAB processed $CsPbBr_3$ thin films. In particular, for the 1.0 mmol PDAB processed thin

145   film, the absorption above 400 nm completely vanishes, revealing that this thin film is composed

146   of pure second-phase with an absorption around 378 nm. Note that, no PL could be detected for

147   this second-phase composed thin film (Figures 1b and S3). Therefore, the sharp absorption peak

148   around 378 nm does not contribute to the PL emission in blue color region as observed in Figure

149   1b, and the corresponding second-phase is classified as one kind of the unnecessary by-products.

150   The UV-vis absorption peak around 378 nm has been observed in reference.For example, when

151   Subila et.al. adopted some ammonium ligands to exfoliate out the fragments of ligand$^+$-[PbBr$_3^-$]

152   complexes from CsPbBr$_3$ nanocrystals, the dominated UV-vis absorption around 320 nm occured,

153   accompanied by the phase transformation of CsPbBr$_3$ nanocrystals into crystalline CsPb$_2$Br$_5$ 2D

154   nanosheets with a lower dimensionality.[41] Along with this, an absorption shoulder peak around

155   380 nm also occurred, and its phase was not affirmed in the mixture system. In other reports of

156   CsPb$_2$Br$_5$ 2D nanosheets or single crystals with relatively simplified phase environment, no sharp

157   absorption peak around 378 nm was observed.[42-44] Thus the sharp absorption peak around 378 nm

158   in our system may not correspond to the CsPb$_2$Br$_5$ perovskite phase. More solid evidence is

159   provided by XRD characterization for the 0.8 mmol and 1.0 mmol PDAB processed thin films. In

160   Figure S4, no peaks corresponding to CsPb$_2$Br$_5$ occur. Particularly, for the 1.0 mmol PDAB

161   processed thin film, even no any XRD peak is detected (Figure S4), which demonstrates that no

162   long-range orderly crystal structure (e.g., CsPbBr$_3$, CsPb$_2$Br$_5$, Cs$_4$PbBr$_6$) dominates in this second-

163   phase composed thin film. Thereby, the experimental evidences of UV-vis absorption (e.g., sharp

164   absorption peak around 378 nm), PL (no PL emission) and XRD results (no obvious crystal

165   structures) exclude the possibility that the second-phase corresponds to any known perovskite

166   crystal phases, such as CsPb$_2$Br$_5$ and Cs$_4$PbBr$_6$.[42-46] In addition, the sharp absorption peak around

167   378 nm is much blue-shifted than that of monolayer A$_2$Cs$_{n-1}$Pb$_n$Br$_{3n+1}$ (n = 1) quantum-well around

168   405 nm in UV-vis spectrum.[14, 23] Overall, all the evidences point to that the second phase

169   corresponds to nanosized molecular clusters (also called as nanoclusters, molecular clusters or

170   magic size clusters),[47-50] namely Cs-Pb-Br-PDAB nanoclusters. The nanoclusters, which are

171   similar to regular nanocrystals but smaller in size (usually < ~1.5 nm), are widely observed with

172   sharp high-energy UV-vis absorption in classical colloidal QDs system.[47-50] Unfortunately, beyond

173   few methods such as UV-vis spectrum, synchrotron technology, etc.,[51] most conventional

174   laboratory methods are difficult to identify the nanoclusters experimentally. The exact composition

175   of the nanoclusters is not further identified in this report; indeed, this second-phase is classified as

176   one kind of the unnecessary by-products, which needs to be avoided. We would highlight more on

177   how to inhibit their formation in our report, which is discussed below.

178   On the other hand, as mentioned above, the incorporation of PDAB ligands into the films would

179   enhance their PL intensity through defect reduction. However, when an excessive amount of

180   PDAB ligands (e.g., 0.8 mmol) were incorporated, the PL intensity decreased. Two main reasons

181   are proposed to explain this observation. First, nonluminous by-products (i.e., nanoclusters) are

182   formed instead of the desired $CsPbBr_3$ QDs when more PDAB ligands are introduced. Second, the

183   particle size of $CsPbBr_3$ QDs decreases when more PDAB ligands are incorporated. When the

184   ligand concentration was increased to 0.8 mmol, the PL spectrum showed further blue-shift, which

185   is due to the quantum confinement effect when the particle size gets smaller. As the size of $CsPbBr_3$

186   QDs decreases, the surface to volume ratio increases, which can introduce more surface defects.[13,]

187   [23] As a consequence, these defects reduce the PL intensity, which has also been observed in 2D

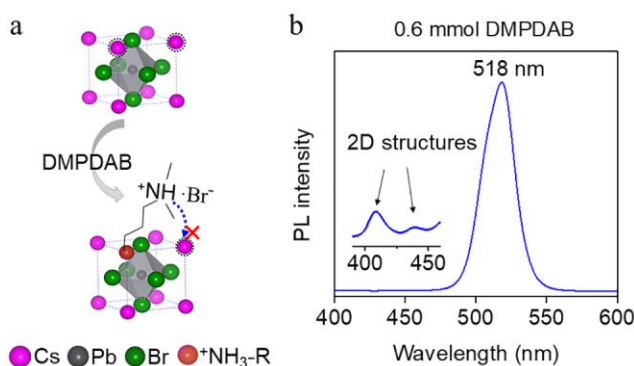188   perovskite structures[13] and classical QD systems.[52]

189

Figure 2. Control experiment using DMPDAB as ligands. (a) Schematic illustration showing that the primary and tertiary ammonium groups of one DMPDAB molecule are difficult to synergistically coordinate with $CsPbBr_3$. (b) PL spectrum of 0.6 mmol DMPDAB processed $CsPbBr_3$ thin films. Inset is a partial enlarged figure evidencing formation of quasi-2D structures.

The enhanced passivation of PDAB is proposed to be induced by its quasi-bidentate coordination with $CsPbBr_3$, in which the two primary ammonium groups of PDAB synergistically occupy around the locations of two adjacent Cs^+ lattice sites of $CsPbBr_3$ (Figures 1d and S5). To verify this, a control experiment was performed using N,N-dimethyl-1,3-propanediamine dihydrobromide (DMPDAB) as ligands (Figure 2). DMPDAB consists of a primary ammonium group and a tertiary ammonium group (Figure 2a). The former is expected to interact with the perovskite structure easily similar to PDAB. However, considering the Goldschmidt tolerance factor,[53-54] the size of the tertiary ammonium group is too large to fit in the crystal structure to stabilize the $PbBr_6^{4-}$ octahedra as reported earlier.[55] Therefore, it is proposed that DMPDAB would not passivate the perovskite structure as effectively as PDAB, because PDAB has two primary ammonium groups participating in the coordination. In addition, the opposite "free" tertiary ammonium groups of DMPDAB may tend to stack via electrostatic interactions, hydrogen bonds or other kinds of polar interactions in the process of crystal formation. This proposal is supported by the formation of quasi-2D perovskites for the DMPDAB processed thin film (Figure S6). Furthermore, no obvious PL blue-shift is detected in this system (Figure 2b), which further suggests the importance of ligand engineering in the $CsPbBr_3$ QDs system. Thus, the synergistic coordination of two primary ammonium groups of PDAB contributes to its enhanced passivation with $CsPbBr_3$. Due to the fully utilized/coordinated functional ammonium groups of the PDAB

11

212   ligands, no stack structures namely 2D perovskites could be formed in the PDAB processed thin

213   films.

214

Figure 3. Mix-ligand (PDAB and PEAB) assisted formation of $CsPbBr_3$ QD films. (a) Molecular

structures of PDAB and PEAB. (b) PL and (c) UV-vis spectra of $CsPbBr_3$ QD films processed by

mixed PDAB and PEAB ligands. The PL curves of 0.6:0- and 0.8:0- $CsPbBr_3$-QD-films are also

integrated in (b). The PL curves in (b) are normalized by the maximal PL intensity of $CsPbBr_3$ thin

films processed with 1.2 mmol of PEAB. (d) Schematic illustration of possible passivation pattern

of PDAB and PEAB on $CsPbBr_3$.

221   PDAB is effective in forming $CsPbBr_3$ QDs with simultaneous PL blue-shift and intensity

222   enhancement, but excessive PDAB induces the formation of nanoclusters and decreases the PL

223   intensity (Figure 1b-c). To avoid that, we intended to weaken the strong passivation effect of

224   PDAB by introducing another competitor with a single ammonium ligand, namely PEAB (Figure

225   3a). Control experiments were performed taking into account the same total molar amounts of

226   ligands for PDAB only or the mixed ligands of PDAB and PEAB. For the 0.6 mmol of ligand

12

227 usage, the PL spectrum of the $CsPbBr_3$ thin film processed with 0.5 mmol PDAB and 0.1 mmol

228 PEAB (marked as 0.5:0.1-$CsPbBr_3$-QD-film) shows almost no peak shift in comparison with that

229 of the film processed with 0.6 mmol PDAB, while the intensity is enhanced (Figure 3b). In

230 addition, the absorption around 378 nm is greatly inhibited (Figure 3c). The inhibition effect for

231 nanocluster formation via mixed ligands of PDAB and PEAB is more obvious upon comparing

232 the absorption around 378 nm for 0.5:0.3- and 0.8:0-$CsPbBr_3$-QD-film (Figures 1c and 3c), while

233 there still exists slight clusters absorption for the 0.5:0.3-$CsPbBr_3$-QD-film around 378 nm. The

234 PL wavelengths exhibit a result of 0.5:1 ≈ 0.6:0, 0.5:0.3 ≈ 0.8:0, indicating that the two systems

235 with the same total molar amounts of ligands emerge with similar partice size, respectively.

236 However, the PL relative intensities exhibit a result of 0.5:1 > 0.6:0, 0.5:0.3 > 0.8:0, respectively.

237 Thus, better optical performance of $CsPbBr_3$ QD films is obtained via the mixed ligand system in

238 comparison with the single PDAB ligand system. On the other hand, for both the single and mixed

239 ligand systems, 0.8 mmol of total ligand usage (0.5:0.3 and 0.8:0) would lead to more blue-shifted

240 emission wavelength, which corresponds to a smaller particle size, than 0.6 mmol of total ligand

241 usage (0.5:0.1 and 0.6:0). The decrease of PL intensity with 0.8 mmol of total ligand usage may

242 be also associated with the increased surface-volume ratio and defects or the formation of

243 nonluminous by-product, as discussed above. Besides, no 2D perovskite structures are formed for

244 the mixed ligands processed thin films (Figures 3b-c and S4). A possible passivation form for the

245 mixed PDAB and PEAB ligand system is proposed in Figure 3d, which shows the co-existing

246 coordination of positive single- and di- ammonium groups with the negative bromide ions.

247 It's known that humidity affects the crystallization and stability of perovskites.[56-57] Considering

248 this, we further studied the humidity's influence on our films (Figures 4, S7-9 and Table S1). One

249 typical example for 0.5:0.1-$CsPbBr_3$-QD-film is provided in Figure 4. Once exposed in air, all the

250   PDAB-contained CsPbBr$_3$ thin films show a gradual PL red-shift, accompanied by a narrowing of

251   peak FWHM, which is consistent with the red-shifted UV-vis absorption spectra (Figures 4a-b,

252   S7-8). Considering the quantum confinement effect, the red-shift phenomenon reveals the size

253   increase of CsPbBr$_3$ QDs, which is further demonstrated by transmission electron microscope

254   (TEM) characterization (Figure 4c). The size of CsPbBr$_3$ QDs could be increased from 5.1 nm to

255   10.0 nm approximately before and after 30 min air exposure. Actually, the PL intensity would be

256   greatly enhanced within a short time of air exposure. This observation is important to achieve a

257   brighter emission from the CsPbBr$_3$ QD film. Moreover, the PL red-shift emerges with the

258   character of continuous change (Figure S7), implying the size tunability of CsPbBr$_3$ QDs. Thus,

259   the influence of humidity turns to be an effective method to realize the size control and color

260   tunability of CsPbBr$_3$ QDs via simple control of exposure time in air, which is regarded as an aging

261   treatment in ambient.
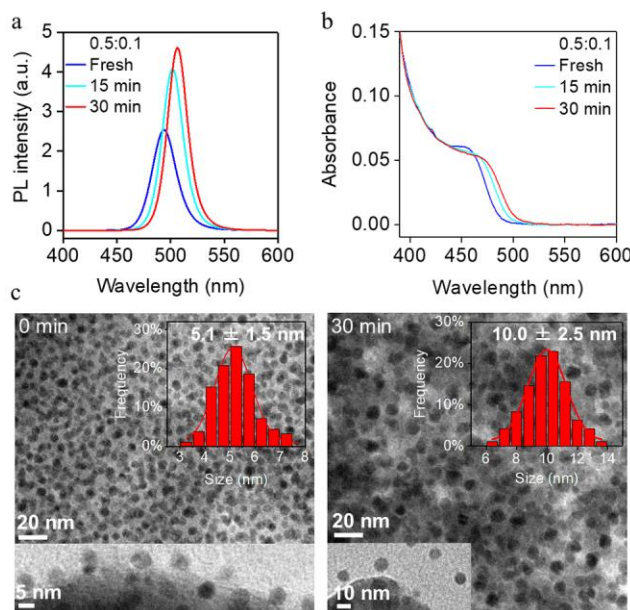

262

263   **Figure 4.** Second growth of CsPbBr$_3$ QDs in 0.5:0.1-CsPbBr$_3$-QD-film upon air exposure (34 ~

264   37% relative humidity (RH)), characterized by (a) PL, (b) UV-vis, and (c) TEM respectively. The

14

PL curves in (a) are normalized by the maximal PL intensity of the 1.2 mmol PEAB processed CsPbBr$_3$ thin film. The "fresh" sample corresponds to the measurement immediately after exposed in air. The histograms of size distribution in (c) are based on the statistic information of ~ 200 particles (0 min) and 100 particles (30 min), respectively.
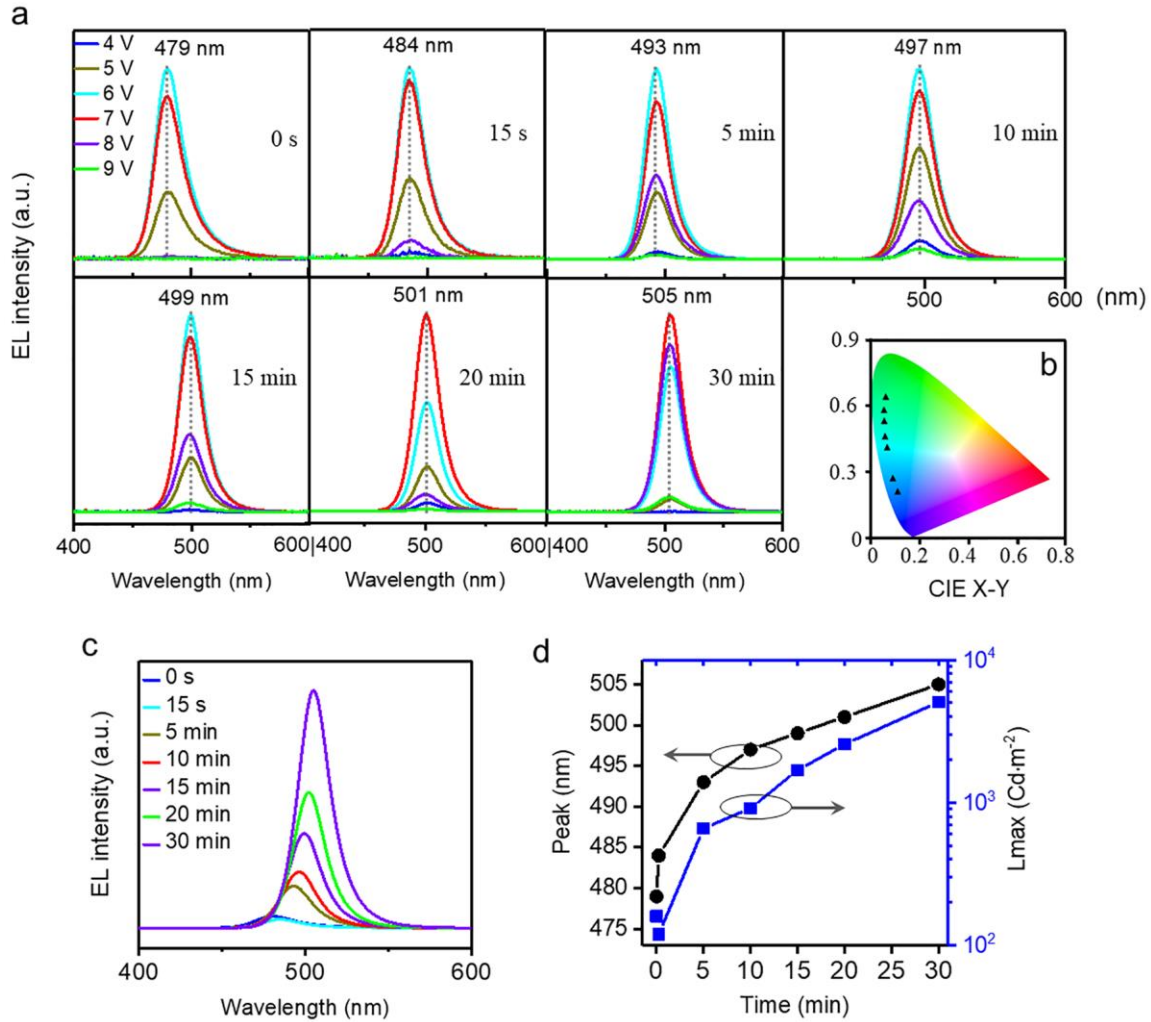

Figure 5. Evolution of EL of the 0.5:0.1-CsPbBr$_3$-QD-films. (a) EL spectra recorded at various applied voltages (4 V – 9 V). The spectral changes at different aging times (0 s – 30 min) and the corresponding peak emission wavelengths are presented in different panels. The films were aged in ambient (34 ~ 37% RH and room temperature) for different times (0 s – 30 min) prior to thermal

274   evaporation. (b) Commission Internationale de l'Éclairage (CIE) values of the EL spectra of

275   0.5:0.1-$CsPbBr_3$-QD-films with various aging time in air. (c) Overall comparison of max EL

276   curves and (d) the statistic information of peak position and maximal luminance (Lmax) as a

277   function of aging time in air.

278   Indeed, the humidity plays an important role for the second-growth phenomenon. Control

279   experiments were performed by storing the 0.5:0.1-$CsPbBr_3$-QD-film in a dry room of 16%

280   relative humidity (RH) and in a N_2 glove box (Figure S9). After 24 h in the dry room, the PL of

281     $CsPbBr_3$ thin film only red-shifts to 500 nm, while the storage in ambient for 24 h results in the

282   emission at 520 nm, which is same as bulk $CsPbBr_3$. Thus, the red-shift phenomenon could be

283   greatly inhibited by decreasing the humidity. This conclusion is further supported by the result of

284   control sample after one-month storage in a N_2 glove box, which showed no red-shift phenomenon.

285   The ammonium group shows a polar character which favors adsorption of moisture in air. Upon

286   air exposure, the polar ammonium ligands undergo a partial solvation at the surface,[58] which

287   induces a second crystal growth of the $CsPbBr_3$ QDs through the Ostwald ripening process.

288   Accompanied by the size increase, the $CsPbBr_3$ QDs may also experience a so-called "self-

289   healing" process of the perovskite lattice in ambient air as reported.[58] For example, Snaith and

290   coworkers have reported that the exposure to moisture could enhance the PL intensity of perovskite

291   film due to partial solvation of the ammonium component and "self-healing" of the perovskite

292   lattice.[58] A recent study by Stranks and coworkers reveals that O_2/H_2O in atmosphere under light

293   soaking may help remove the trap states at the perovskite surface,[59] thus an enhanced PL intensity

294   could be obtained within short-time exposure in air.

295   EL studies were performed taking the 0.5:0.1-$CsPbBr_3$-QD-films as an example. As discussed

296   above, continuously tunable emissions for the thin films can be achieved via simple control of

297   exposure time in air. With this consideration, the thin films were firstly treated by aging in ambient

298   (34 ~ 37% RH and room temperature) for 0 s - 30 min, respectively. The CsPbBr$_3$ QD films exhibit

299   smooth surface roughness within the exposure period in ambient (Figure S10). Notably, no Pb^0 is

300   observed for the thin films after aging treatment (Figure S11). In the subsequent step, electron

301   injection layer 4,6-Bis(3,5-di(pyridin-3-yl)phenyl)-2-methylpyrimidine (B$_3$PYMPM) and LiF/Al

302   electrode were sequentially evaporated onto the CsPbBr$_3$ QD films in high vacuum (Figure S12).

303   The EL properties were evaluated directly in air. The samples with various aging time exhibit

304   continuously tunable emissions in EL spectra (Figure 5), from 479 nm (0 s) to 505 nm (30 min),

305   respectively. Accompanied by the EL wavelength changes, the EL emission intensity is also

306   enhanced with the luminance increasing from 165 Cd/m^2 (at 479 nm, 0 s) to 5058 Cd/m^2 (at 505

307   nm, 30 min) as shown in Figure 5b-c. For each sample with the exact aging time in air, the EL

308   spectra do not show any shift under various voltage biases, which obviously differ from the results

309   in mixed halide system as reported.[13, 19] On the other hand, this result also demonstrates that the

310   evaporation process of organic electron transfer material and electrode onto CsPbBr$_3$ QD films can

311   inhibit the direct influence of humidity upon the size change of CsPbBr$_3$ QDs.

312   In summary, for the first time, we successfully developed a new CsPbBr$_3$ QD film system via one-

313   step spin-coating route that differs from the traditional colloidal synthesis route. The PDAB

314   ligands were found to efficiently inhibit the crystal growth of CsPbBr$_3$ QDs. The mixed ligand

315   system of PDAB and PEAB was further developed to enhance their emission properties. The

316   CsPbBr$_3$ QDs showed a second growth process in air, which provided another feasible way to

317   realize the size control of CsPbBr$_3$ QDs via simple control of aging time in air. As a result,

318   continuously tunable emissions from green to blue colors were achieved in the PL and EL spectra.

319   Importantly, the produced CsPbBr$_3$ QD films demonstrate no spectra-drift in EL upon voltage bias.

320 These results are expected to accelerate the exploration of blue-emitting applications of
321 perovskites.

322 ASSOCIATED CONTENT

323 **Supporting Information**

324 The Supporting Information is available free of charge on the ACS Publications website at
325 DOI:xxxxx.

326   Chemicals, film/device fabrication procedures, characterization method; additional
327   discussion; PL, PL lifetime, XRD, UV-vis, AFM, X-ray photoelectron spectroscopy (XPS)
328   and EL (PDF)

329 AUTHOR INFORMATION

330 **Corresponding Author**

331 *Yabing Qi, E-Mail: Yabing.Qi@OIST.jp

332 **ORCID**

333 Maowei Jiang: 0000-0001-8364-2938

334 Zhanhao Hu: 0000-0002-2892-6388

335 Zonghao Liu: 0000-0003-4743-6971

336 Luis K. Ono: 0000-0003-3176-1876

337 Yabing Qi: 0000-0002-4876-8049

338 **Author contributions**

339　M. J. and Z. H. contributed equally to this work.

340　**Notes**

341　The authors declare no competing financial interest.

347　**REFERENCES**

348　 (1) Lee, M. M.; Teuscher, J.; Miyasaka, T.; Murakami, T. N.; Snaith, H. J. Efficient Hybrid

349　Solar Cells Based on Meso-Superstructured Organometal Halide Perovskites. *Science* **2012,** *338*,

350　643-647.

351　 (2) Tan, Z. K.; Moghaddam, R. S.; Lai, M. L.; Docampo, P.; Higler, R.; Deschler, F.; Price, M.;

352　Sadhanala, A.; Pazos, L. M.; Credgington, D.; Hanusch, F.; Bein, T.; Snaith, H. J.; Friend, R. H.

353　Bright Light-Emitting Diodes Based on Organometal Halide Perovskite. *Nat. Nanotechnol.* **2014,**

354　*9*, 687-692.

355　 (3) Dou, L. T.; Yang, Y.; You, J. B.; Hong, Z. R.; Chang, W. H.; Li, G.; Yang, Y. Solution-

356　Processed Hybrid Perovskite Photodetectors with High Detectivity. *Nat. Commun.* **2014,** *5*,

357　5404.

358　 (4) Wang, Y.; Li, X.; Song, J.; Xiao, L.; Zeng, H.; Sun, H. All-Inorganic Colloidal Perovskite

359　Quantum Dots: A New Class of Lasing Materials with Favorable Characteristics. *Adv. Mater.*

360　**2015,** *27*, 7101-7108.

361　 (5) Li, C.; Han, C.; Zhang, Y.; Zang, Z.; Wang, M.; Tang, X.; Du, J. Enhanced Photoresponse of

362　Self-Powered Perovskite Photodetector Based on ZnO Nanoparticles Decorated CsPbBr3 Films.

363　*Sol. Energy Mater. Sol. Cells* **2017,** *172*, 341-346.

364 (6) Lin, K.; Xing, J.; Quan, L. N.; de Arquer, F. P. G.; Gong, X.; Lu, J.; Xie, L.; Zhao, W.;

365 Zhang, D.; Yan, C.; Li, W.; Liu, X.; Lu, Y.; Kirman, J.; Sargent, E. H.; Xiong, Q.; Wei, Z.

366 Perovskite Light-Emitting Diodes with External Quantum Efficiency Exceeding 20 Per Cent.

367 *Nature* **2018,** *562*, 245-248.

368 (7) Cao, Y.; Wang, N. N.; Tian, H.; Guo, J. S.; Wei, Y. Q.; Chen, H.; Miao, Y. F.; Zou, W.; Pan,

369 K.; He, Y. R.; Cao, H.; Ke, Y.; Xu, M. M.; Wang, Y.; Yang, M.; Du, K.; Fu, Z. W.; Kong, D. C.;

370 Dai, D. X.; Jin, Y. Z.; Li, G. Q.; Li, H.; Peng, Q. M.; Wang, J. P.; Huang, W. Perovskite Light-

371 Emitting Diodes Based on Spontaneously Formed Submicrometre-Scale Structures. *Nature*

372 **2018,** *562*, 249-253.

373 (8) Zhao, B. D.; Bai, S.; Kim, V.; Lamboll, R.; Shivanna, R.; Auras, F.; Richter, J. M.; Yang, L.;

374 Dai, L. J.; Alsari, M.; She, X. J.; Liang, L. S.; Zhang, J. B.; Lilliu, S.; Gao, P.; Snaith, H. J.;

375 Wang, J. P.; Greenham, N. C.; Friend, R. H.; Di, D. W. High-Efficiency Perovskite-Polymer

376 Bulk Heterostructure Light-Emitting Diodes. *Nat. Photon.* **2018,** *12*, 783-789.

377 (9) Cho, H. C.; Jeong, S. H.; Park, M. H.; Kim, Y. H.; Wolf, C.; Lee, C. L.; Heo, J. H.;

378 Sadhanala, A.; Myoung, N.; Yoo, S.; Im, S. H.; Friend, R. H.; Lee, T. W. Overcoming the

379 Electroluminescence Efficiency Limitations of Perovskite Light-Emitting Diodes. *Science* **2015,**

380 *350*, 1222-1225.

381 (10) Xu, W.; Hu, Q.; Bai, S.; Bao, C.; Miao, Y.; Yuan, Z.; Borzda, T.; Barker, A. J.; Tyukalova,

382 E.; Hu, Z.; Kawecki, M.; Wang, H.; Yan, Z.; Liu, X.; Shi, X.; Uvdal, K.; Fahlman, M.; Zhang,

383 W.; Duchamp, M.; Liu, J.-M.; Petrozza, A.; Wang, J.; Liu, L.-M.; Huang, W.; Gao, F. Rational

384 Molecular Passivation for High-Performance Perovskite Light-Emitting Diodes. *Nat. Photon.*

385 **2019,** *13*, 418–424.

386 (11) Kumar, S.; Jagielski, J.; Yakunin, S.; Rice, P.; Chiu, Y. C.; Wang, M. C.; Nedelcu, G.;

387 Kim, Y.; Lin, S. C.; Santos, E. J. G.; Kovalenko, M. V.; Shih, C. J. Efficient Blue

388 Electroluminescence Using Quantum-Confined Two-Dimensional Perovskites. *ACS Nano* **2016,**

389 *10*, 9720-9729.

390 (12) Liu, Y.; Cui, J.; Du, K.; Tian, H.; He, Z.; Zhou, Q.; Yang, Z.; Deng, Y.; Chen, D.; Zuo, X.;

391 Ren, Y.; Wang, L.; Zhu, H.; Zhao, B.; Di, D.; Wang, J.; Friend, R. H.; Jin, Y. Efficient Blue

392 Light-Emitting Diodes Based on Quantum-Confined Bromide Perovskite Nanostructures. *Nat.*

393 *Photon.* **2019**, Doi:10.1038/s41566-019-0505-4.

394   (13) Li, Z.; Chen, Z.; Yang, Y.; Xue, Q.; Yip, H.-L.; Cao, Y. Modulation of Recombination

395   Zone Position for Quasi-Two-Dimensional Blue Perovskite Light-Emitting Diodes with

396   Efficiency Exceeding 5%. *Nat. Commun.* **2019,** *10*, 1027.

397   (14) Xing, J.; Zhao, Y.; Askerka, M.; Quan, L. N.; Gong, X.; Zhao, W.; Zhao, J.; Tan, H.; Long,

398   G.; Gao, L.; Yang, Z.; Voznyy, O.; Tang, J.; Lu, Z.-H.; Xiong, Q.; Sargent, E. H. Color-Stable

399   Highly Luminescent Sky-Blue Perovskite Light-Emitting Diodes. *Nat. Commun.* **2018,** *9*, 3541.

400   (15) Li, G.; Rivarola, F. W. R.; Davis, N. J. L. K.; Bai, S.; Jellicoe, T. C.; de la Peña, F.; Hou,

401   S.; Ducati, C.; Gao, F.; Friend, R. H.; Greenham, N. C.; Tan, Z.-K. Highly Efficient Perovskite

402   Nanocrystal Light-Emitting Diodes Enabled by a Universal Crosslinking Method. *Adv. Mater.*

403   **2016,** *28*, 3528-3534.

404   (16) Gangishetty, M. K.; Hou, S. C.; Quan, Q. M.; Congreve, D. N. Reducing Architecture

405   Limitations for Efficient Blue Perovskite Light-Emitting Diodes. *Adv. Mater.* **2018,** *30*, 1706226.

406   (17) Yao, E. P.; Yang, Z. L.; Meng, L.; Sun, P. Y.; Dong, S. Q.; Yang, Y.; Yang, Y. High-

407   Brightness Blue and White Leds Based on Inorganic Perovskite Nanocrystals and Their

408   Composites. *Adv. Mater.* **2017,** *29*, 1606859.

409   (18) Song, J. Z.; Li, J. H.; Li, X. M.; Xu, L. M.; Dong, Y. H.; Zeng, H. B. Quantum Dot Light-

410   Emitting Diodes Based on Inorganic Perovskite Cesium Lead Halides (CsPbX3). *Adv. Mater.*

411   **2015,** *27*, 7162-7167.

412   (19) Vashishtha, P.; Ng, M.; Shivarudraiah, S. B.; Halpert, J. E. High Efficiency Blue and Green

413   Light-Emitting Diodes Using Ruddlesden–Popper Inorganic Mixed Halide Perovskites with

414   Butylammonium Interlayers. *Chem. Mater.* **2019,** *31*, 83-89.

415   (20) Xiao, Z. G.; Kerner, R. A.; Zhao, L. F.; Tran, N. L.; Lee, K. M.; Koh, T. W.; Scholes, G.

416   D.; Rand, B. P. Efficient Perovskite Light-Emitting Diodes Featuring Nanometre-Sized

417   Crystallites. *Nat. Photon.* **2017,** *11*, 108-115.

418   (21) Yuan, M. J.; Quan, L. N.; Comin, R.; Walters, G.; Sabatini, R.; Voznyy, O.; Hoogland, S.;

419   Zhao, Y. B.; Beauregard, E. M.; Kanjanaboos, P.; Lu, Z. H.; Kim, D. H.; Sargent, E. H.

420   Perovskite Energy Funnels for Efficient Light-Emitting Diodes. *Nat. Nanotechnol.* **2016,** *11*,

421   872-877.

422   (22) Shang, Y. Q.; Li, G.; Liu, W. M.; Ning, Z. J. Quasi-2D Inorganic CsPbBr3 Perovskite for

423   Efficient and Stable Light-Emitting Diodes. *Adv. Funct. Mater.* **2018,** *28*, 1801193.

424   (23) Yang, X. L.; Zhang, X. W.; Deng, J. X.; Chu, Z. M.; Jiang, Q.; Meng, J. H.; Wang, P. Y.;

425   Zhang, L. Q.; Yin, Z. G.; You, J. B. Efficient Green Light-Emitting Diodes Based on Quasi-

426   Two-Dimensional Composition and Phase Engineered Perovskite with Surface Passivation. *Nat.*

427   *Commun.* **2018,** *9*, 570.

428   (24) Si, J.; Liu, Y.; He, Z.; Du, H.; Du, K.; Chen, D.; Li, J.; Xu, M.; Tian, H.; He, H.; Di, D.;

429   Lin, C.; Cheng, Y.; Wang, J.; Jin, Y. Efficient and High-Color-Purity Light-Emitting Diodes

430   Based on in Situ Grown Films of CsPbX3 (X = Br, I) Nanoplates with Controlled Thicknesses.

431   *ACS Nano* **2017,** *11*, 11100-11107.

432   (25) Protesescu, L.; Yakunin, S.; Bodnarchuk, M. I.; Krieg, F.; Caputo, R.; Hendon, C. H.;

433   Yang, R. X.; Walsh, A.; Kovalenko, M. V. Nanocrystals of Cesium Lead Halide Perovskites

434   (CsPbX3, X = Cl, Br, and I): Novel Optoelectronic Materials Showing Bright Emission with

435   Wide Color Gamut. *Nano Lett.* **2015,** *15*, 3692-3696.

436   (26) Dong, Y. T.; Qiao, T.; Kim, D.; Parobek, D.; Rossi, D.; Son, D. H. Precise Control of

437   Quantum Confinement in Cesium Lead Halide Perovskite Quantum Dots Via Thermodynamic

438   Equilibrium. *Nano Lett.* **2018,** *18*, 3716-3722.

439   (27) Akkerman, Q. A.; Raino, G.; Kovalenko, M. V.; Manna, L. Genesis, Challenges and

440   Opportunities for Colloidal Lead Halide Perovskite Nanocrystals. *Nat. Mater.* **2018,** *17*, 394-405.

441   (28) Yan, D.; Shi, T.; Zang, Z.; Zhou, T.; Liu, Z.; Zhang, Z.; Du, J.; Leng, Y.; Tang, X.

442   Ultrastable CsPbBr3 Perovskite Quantum Dot and Their Enhanced Amplified Spontaneous

443   Emission by Surface Ligand Modification. *Small* **2019,** *15*, 1901173.

444   (29) Song, J.; Fang, T.; Li, J.; Xu, L.; Zhang, F.; Han, B.; Shan, Q.; Zeng, H. Organic–Inorganic

445   Hybrid Passivation Enables Perovskite QLEDs with an EQE of 16.48%. *Adv. Mater.* **2018,** *30*,

446   1805409.

447   (30) Shi, Z. F.; Li, Y.; Zhang, Y. T.; Chen, Y. S.; Li, X. J.; Wu, D.; Xu, T. T.; Shan, C. X.; Du,

448   G. T. High-Efficiency and Air-Stable Perovskite Quantum Dots Light-Emitting Diodes with an

449   All-Inorganic Heterostructure. *Nano Lett.* **2017,** *17*, 313-321.

450   (31) Li, C.; Zang, Z.; Chen, W.; Hu, Z.; Tang, X.; Hu, W.; Sun, K.; Liu, X.; Chen, W. Highly

451   Pure Green Light Emission of Perovskite CsPbBr3 Quantum Dots and Their Application for

452   Green Light-Emitting Diodes. *Opt. Express* **2016,** *24*, 15071-15078.

453   (32) Liang, Z.; Zhao, S.; Xu, Z.; Qiao, B.; Song, P.; Gao, D.; Xu, X. Shape-Controlled Synthesis

454   of All-Inorganic CsPbBr3 Perovskite Nanocrystals with Bright Blue Emission. *Acs Appl. Mater.*

455   *Interfaces* **2016,** *8*, 28824-28830.

456   (33) Dutta, A.; Dutta, S. K.; Das Adhikari, S.; Pradhan, N. Tuning the Size of CsPbBr3

457   Nanocrystals: All at One Constant Temperature. *ACS Energy Lett.* **2018,** *3*, 329-334.

458   (34) Brennan, M. C.; Herr, J. E.; Nguyen-Beck, T. S.; Zinna, J.; Draguta, S.; Rouvimov, S.;

459   Parkhill, J.; Kuno, M. Origin of the Size-Dependent Stokes Shift in CsPbBr3 Perovskite

460   Nanocrystals. *J. Am. Chem. Soc.* **2017,** *139*, 12201-12208.

461   (35) Chiba, T.; Hoshi, K.; Pu, Y. J.; Takeda, Y.; Hayashi, Y.; Ohisa, S.; Kawata, S.; Kido, J.

462   High-Efficiency Perovskite Quantum-Dot Light-Emitting Devices by Effective Washing Process

463   and Interfacial Energy Level Alignment. *Acs Appl. Mater. Interfaces* **2017,** *9*, 18054-18060.

464   (36) Li, J. H.; Xu, L. M.; Wang, T.; Song, J. Z.; Chen, J. W.; Xue, J.; Dong, Y. H.; Cai, B.;

465   Shan, Q. S.; Han, B. N.; Zeng, H. B. 50-Fold EQE Improvement up to 6.27% of Solution-

466   Processed All-Inorganic Perovskite CsPbBr3 QLEDs Via Surface Ligand Density Control. *Adv.*

467   *Mater.* **2017,** *29*, 1603885.

468   (37) Kim, Y. H.; Wolf, C.; Kim, Y. T.; Cho, H.; Kwon, W.; Do, S.; Sadhanala, A.; Park, C. G.;

469   Rhee, S. W.; Im, S. H.; Friend, R. H.; Lee, T. W. Highly Efficient Light-Emitting Diodes of

470   Colloidal Metal-Halide Perovskite Nanocrystals Beyond Quantum Size. *ACS Nano* **2017,** *11*,

471   6586-6593.

472   (38) Zhang, L. Q.; Yang, X. L.; Jiang, Q.; Wang, P. Y.; Yin, Z. G.; Zhang, X. W.; Tan, H. R.;

473   Yang, Y.; Wei, M. Y.; Sutherland, B. R.; Sargent, E. H.; You, J. B. Ultra-Bright and Highly

474   Efficient Inorganic Based Perovskite Light-Emitting Diodes. *Nat. Commun.* **2017,** *8*, 15640.

475   (39) Wu, Y.; Wei, C. T.; Li, X. M.; Li, Y. L.; Qiu, S. C.; Shen, W.; Cai, B.; Sun, Z. G.; Yang, D.

476   D.; Deng, Z. T.; Zeng, H. B. In Situ Passivation of PbBr$_6^{4-}$ Octahedra toward Blue Luminescent

477   CsPbBr3 Nanoplatelets with near 100% Absolute Quantum Yield. *ACS Energy Lett.* **2018,** *3*,

478   2030-2037.

479   (40) Butkus, J.; Vashishtha, P.; Chen, K.; Gallaher, J. K.; Prasad, S. K. K.; Metin, D. Z.;

480   Laufersky, G.; Gaston, N.; Halpert, J. E.; Hodgkiss, J. M. The Evolution of Quantum

481   Confinement in CsPbBr3 Perovskite Nanocrystals. *Chem. Mater.* **2017,** *29*, 3644-3652.

482   (41) Balakrishnan, S. K.; Kamat, P. V. Ligand Assisted Transformation of Cubic CsPbBr3

483   Nanocrystals into Two-Dimensional CsPb2Br5 Nanosheets. *Chem. Mater.* **2018,** *30*, 74-78.

484   (42) Li, G.; Wang, H.; Zhu, Z.; Chang, Y.; Zhang, T.; Song, Z.; Jiang, Y. Shape and Phase

485   Evolution from CsPbBr3 Perovskite Nanocubes to Tetragonal CsPb2Br5 Nanosheets with an

486   Indirect Bandgap. *Chem. Commun.* **2016,** *52*, 11296-11299.

487   (43) Wang, K.-H.; Wu, L.; Li, L.; Yao, H.-B.; Qian, H.-S.; Yu, S.-H. Large-Scale Synthesis of

488   Highly Luminescent Perovskite-Related CsPb2Br5 Nanoplatelets and Their Fast Anion

489   Exchange. *Angew. Chem. Int. Ed.* **2016,** *55*, 8328-8332.

490   (44) Dursun, I.; De Bastiani, M.; Turedi, B.; Alamer, B.; Shkurenko, A.; Yin, J.; El-Zohry, A.

491   M.; Gereige, I.; AlSaggaf, A.; Mohammed, O. F.; Eddaoudi, M.; Bakr, O. M. CsPb2Br5 Single

492   Crystals: Synthesis and Characterization. *ChemSusChem* **2017,** *10*, 3746-3749.

493   (45) Saidaminov, M. I.; Almutlaq, J.; Sarmah, S.; Dursun, I.; Zhumekenov, A. A.; Begum, R.;

494   Pan, J.; Cho, N.; Mohammed, O. F.; Bakr, O. M. Pure Cs4PbBr6: Highly Luminescent Zero-

495   Dimensional Perovskite Solids. *ACS Energy Lett.* **2016,** *1*, 840-845.

496   (46) Liu, Z. K.; Bekenstein, Y.; Ye, X. C.; Nguyen, S. C.; Swabeck, J.; Zhang, D. D.; Lee, S. T.;

497   Yang, P. D.; Ma, W. L.; Alivisatos, A. P. Ligand Mediated Transformation of Cesium Lead

498   Bromide Perovskite Nanocrystals to Lead Depleted Cs4PbBr6 Nanocrystals. *J. Am. Chem. Soc.*

499   **2017,** *139*, 5309-5312.

500   (47) Alivisatos, A. P. Semiconductor Clusters, Nanocrystals, and Quantum Dots. *Science* **1996,**

501   *271*, 933-937.

502   (48) Xie, R.; Li, Z.; Peng, X. Nucleation Kinetics Vs Chemical Kinetics in the Initial Formation

503   of Semiconductor Nanocrystals. *J. Am. Chem. Soc.* **2009,** *131*, 15457-15466.

504   (49) Gary, D. C.; Flowers, S. E.; Kaminsky, W.; Petrone, A.; Li, X.; Cossairt, B. M. Single-

505   Crystal and Electronic Structure of a 1.3 nm Indium Phosphide Nanocluster. *J. Am. Chem. Soc.*

506   **2016,** *138*, 1510-1513.

507   (50) Li, J.; Wang, H.; Lin, L.; Fang, Q.; Peng, X. Quantitative Identification of Basic Growth

508   Channels for Formation of Monodisperse Nanocrystals. *J. Am. Chem. Soc.* **2018,** *140*, 5474-

509   5484.

510   (51) Abécassis, B.; Bouet, C.; Garnero, C.; Constantin, D.; Lequeux, N.; Ithurria, S.; Dubertret,

511   B.; Pauw, B. R.; Pontoni, D. Real-Time in Situ Probing of High-Temperature Quantum Dots

512   Solution Synthesis. *Nano Lett.* **2015,** *15*, 2620-2626.

513   (52) Qu, L. H.; Peng, X. G. Control of Photoluminescence Properties of Cdse Nanocrystals in

514   Growth. *J. Am. Chem. Soc.* **2002,** *124*, 2049-2055.

515 (53) Goldschmidt, V. M. Die Gesetze Der Krystallochemie. *Naturwissenschaften* **1926,** *14*, 477-

516 485.

517 (54) Zhou, T. W.; Wang, M.; Zang, Z. G.; Fang, L. Stable Dynamics Performance and High

518 Efficiency of ABX(3)-Type Super-Alkali Perovskites First Obtained by Introducing H5O2

519 Cation. *Adv. Energy Mater.* **2019,** *9*, 1900664.

520 (55) Becker, M.; Klüner, T.; Wark, M. Formation of Hybrid ABX3 Perovskite Compounds for

521 Solar Cell Application: First-Principles Calculations of Effective Ionic Radii and Determination

522 of Tolerance Factors. *Dalton Trans.* **2017,** *46*, 3500-3509.

523 (56) You, J. B.; Yang, Y. M.; Hong, Z. R.; Song, T. B.; Meng, L.; Liu, Y. S.; Jiang, C. Y.; Zhou,

524 H. P.; Chang, W. H.; Li, G.; Yang, Y. Moisture Assisted Perovskite Film Growth for High

525 Performance Solar Cells. *Appl. Phys. Lett.* **2014,** *105*, 183902.

526 (57) Raga, S. R.; Jung, M. C.; Lee, M. V.; Leyden, M. R.; Kato, Y.; Qi, Y. B. Influence of Air

527 Annealing on High Efficiency Planar Structure Perovskite Solar Cells. *Chem. Mater.* **2015,** *27*,

528 1597-1603.

529 (58) Eperon, G. E.; Habisreutinger, S. N.; Leijtens, T.; Bruijnaers, B. J.; van Franeker, J. J.;

530 deQuilettes, D. W.; Pathak, S.; Sutton, R. J.; Grancini, G.; Ginger, D. S.; Janssen, R. A. J.;

531 Petrozza, A.; Snaith, H. J. The Importance of Moisture in Hybrid Lead Halide Perovskite Thin

532 Film Fabrication. *ACS Nano* **2015,** *9*, 9380-9393.

533 (59) Brenes, R.; Eames, C.; Bulović, V.; Islam, M. S.; Stranks, S. D. The Impact of Atmosphere

534 on the Local Luminescence Properties of Metal Halide Perovskite Grains. *Adv. Mater.* **2018,** *30*,

535 1706208.